Shock-wave structure via nonequilibrium molecular dynamics and Navier-Stokes continuum mechanics

Brad Lee Holian

Los Alamos Scientific National Laboratory, Los Alamos, New Mexico 87545

William G. Hoover and Bill Moran

Lawrence Livermore National Laboratory, Livermore, California 94550
and Department of Applied Science, University of California at Davis-Livermore, Livermore, California 94550

Galen K. Straub

Los Alamos Scientific National Laboratory, Los Alamos, New Mexico 87545

A strong steady dense-fluid shock wave is simulated with 4800-atom nonequilibrium molecular dynamics. The resulting density, stress, energy, and temperature profiles are compared with corresponding macroscopic profiles we derive from Navier-Stokes continuum mechanics. The differences found are relatively small.

I. INTRODUCTION

Microscopic fluid transport theory seeks to describe the flows of mass, momentum, and energy due to gradients in chemical potential, stress, and temperature. For small gradients, the flows are "linear", proportional to the gradients. The task of the theory is to identify the coefficients (diffusion coefficient, shear and bulk viscosity, and thermal conductivity) and to describe the limits of the simple linear theory. Macroscopic fluid transport theory begins by assuming, rather than deriving, a "constitutive model" relating flows to gradients. The macroscopic theory is devoted to solving the differential conservation equations for specific boundary conditions. The macroscopic theory should apply best where gradients are small, as in geophysical problems, and should be applied more cautiously when gradients are appreciable on the scale of atoms or microscopic grains.

In this work we consider the large-gradient microscale extreme, a very strong shock wave in a dense atomic fluid. Is it reasonable, or even possible, to treat a strong shock wave, with large gradients, using the small-gradient "Navier-Stokes" theory of macroscopic continuum mechanics? This question has been discussed at length in the literature. Our own view—supported by the results reported here—is that the comparison of fundamental *results*, from experiments or simulations, with the *predictions* of well-defined theories has intrinsic interest.

Shock waves are inherently irreversible, and are usually generated by explosions, or collisions of macroscopic bodies, and, with clever diagnostics, can yield equation-of-state information in regimes of pressure and temperature which are normally inaccessible.[1] The range of pressures obtained in shock-wave compressions is gradually increasing toward the many thousand megabars required for laser-fusion power plants. Liquid argon has been compressed to nearly one megabar,[2] water to more than two megabars,[3] and heavy metals to about 100 megabars.[4]
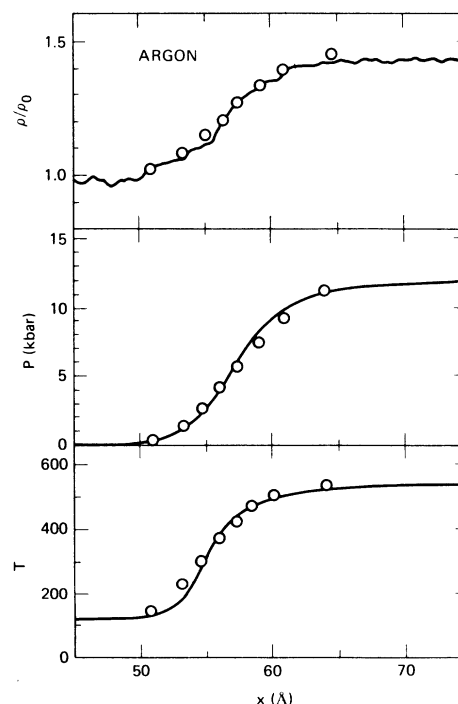

FIG. 1. Comparison of atomistic and Navier-Stokes shock-wave density, pressure, and temperature profiles taken from Ref. 6. The full curves were obtained using nonequilibrium molecular dynamics. The circles are taken from the corresponding continuum calculation.

At pressures and temperatures sufficiently great to ionize the shocked sample, long-range Coulomb interactions dominate the microscopic dynamics. Here we focus on the compression of a classical fluid to avoid the complication of ionization. Because previous work (see Fig. 1) indicated that compressions corresponding to shock-wave pressures of 30 kilobars in argon[5] could be successfully described by the continuum Navier-Stokes equations,[6] we chose to study the strongest possible shock wave for which argon is still not ionized, corresponding to a final temperature of 12 000 K and pressure of nearly 400 kilobars.

The work reported on here is described as follows: Sec. II—Description of shock-wave geometry from the continuum viewpoint; Sec. III—Constitutive characterization of the Lennard-Jones fluid; Sec. IV—Solution of the macroscopic continuum equations within the shock wave; Sec. V—Solution of the microscopic equations of motion within the shock wave; Sec. VI—Comparison of the profiles and nonequilibrium fluxes from IV and V.

II. SHOCK WAVE GEOMETRY

The existence of shock waves and some details of their structure have been established experimentally. It is possible to understand the existence[7] of a steady shock-wave profile in a fluid in terms of two competing processes: The wave tends to steepen due to the higher sound velocity in the shocked material, and the wave tends to spread out due to the extra viscous stress caused by a velocity gradient. Detailed structure calculations indicate that in fluids the shock width resulting from these opposing effects is of order the atomic mean free path.[8] Numerical calculations, using constitutive relations established empirically, corroborate the experimental evidence for shock waves. In the underlying constitutive models, it is necessary that the material have a characteristic microscopic length or frequency (such as the interatomic spacing or the collision rate); a constitutive relation expressing stress solely as a function of strain, without rate dependence, cannot produce a steady shock wave. In the event that a steady profile does exist—or even if the profile is nonsteady but grows less rapidly than linearly in the time—then conservation of mass, momentum, and energy can be used to correlate the thermodynamic states on either side of the shock wave.

The shock-wave geometry is shown from three different points of view in Fig. 2. At the top of the figure a piston with velocity $-u_p$ generates a shock wave running at velocity $-u_s$ into stationary fluid. In the process of accelerating the fluid from rest to the piston velocity, the pressure rises from

P_0 to P_1, the temperature from T_0 to T_1, and the internal energy per unit mass from E_0 to E_1. If we choose instead the coordinate system at the center of Fig. 2, fixed in the shocked material, then the piston is also motionless and the cold unshocked fluid moves to the right at velocity u_p, then stagnates to velocity zero, creating a shock wave running to the left at velocity $u_p - u_s$. A third coordinate system, more useful than the first two, is shown at the bottom of Fig. 2. The fluid streams toward the piston, at velocity u_s, and the piston moves to the right at just the velocity $u_s - u_p$, required to maintain the shock-wave center at the origin. If the shock wave has a steady profile, then, in this last coordinate frame only, the flows of mass, momentum, and energy must have constant values throughout the steady profile:

$$\rho u, \quad P_{xx} + \rho u^2, \quad [E + (P_{xx}/\rho) + \tfrac{1}{2}u^2]\rho u + q ,$$

are all constant for $u_s - u_p \le u \le u_s$. P_{xx} and q $= -\kappa \, dT/dx$ are the fluxes, in the shock (x) direction, of x momentum and energy in a comoving frame of velocity u fixed in the fluid. ρ is the mass density and E is the internal energy (excluding the kinetic energy of mass motion associated with the stream velocity u) per unit mass. If the conserved momentum and energy fluxes are evaluated far from the shock wave, where P_{xx} is equal to the equilibrium (inviscid and isotropic), pressure P and the heat flux q vanishes, then the conservation relations provide three relations among the material properties of the unshocked and shocked
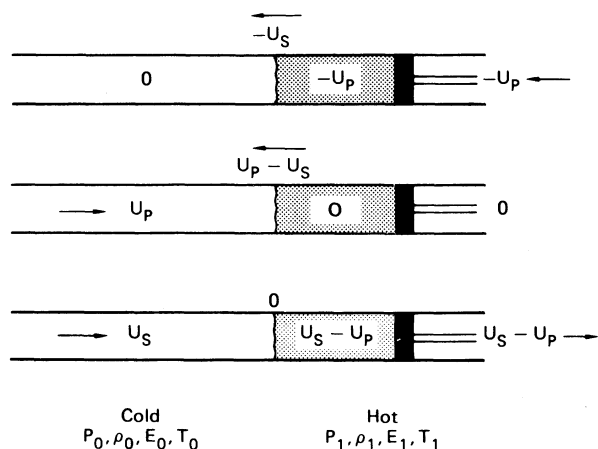

FIG. 2. Steady fluid shock waves viewed in three different coordinate frames. In the topmost frame the piston at the right moves to the left, compressing and heating the cold fluid. In the middle frame the piston is fixed and cold fluid moves to the right. The frame at the bottom of the figure fixed on the shock wave leads to the simple conservation equations solved in the text.

material:

$$\rho_0 u_0 = \rho_1 u_1 ,$$

$$P_0 + \rho_0 u_0^2 = P_1 + \rho_1 u_1^2 , \tag{1}$$

$$E_0 + P_0/\rho_0 + \tfrac{1}{2} u_0^2 = E_1 + P_1/\rho_1 + \tfrac{1}{2} u_1^2 .$$

When the two velocities, $u_0 \equiv u_s$, and $u_1 \equiv u_s - u_p$, are eliminated from (1) the resulting "Hugoniot" relation between the internal energy change and the driving pressures results:

$$E_1 - E_0 = \tfrac{1}{2}(P_0 + P_1)(V_0 - V_1) , \tag{2}$$

where V_0 and V_1 are the volumes per unit mass. The Hugoniot relation (2) can be solved (for the final pressure and energy, P_1 and E_1) when pressure and energy are known functions of density and temperature, by varying the temperature at the final volume V_1 and comparing the two sides of the equation. See Appendix A.

In fluids, shock-wave calculations are relatively straightforward because the initial and final pressures are both isotropic and both internal energies are given by the equilibrium thermodynamic equation of state. In solids[9] one expects to find a residual shear stress in the shocked material. This shear stress, together with its effect on the internal energy, must be included in solving the solid-phase analog of (2).

III. LENNARD-JONES CONSTITUTIVE RELATION

In any comparison of an approximate theory (such as the Navier-Stokes equations) with fundamental results (solutions of Newton's equations of motion) it is essential that the underlying material be well characterized. Computer experiments,[9,10] as opposed to laboratory experiments, can avoid material uncertainties by specifying interatomic forces which are used in both the approximate and the fundamental calculations. A useful representation of fluid properties can be based on the Lennard-Jones potential

$$\phi = 4\epsilon[(\sigma/r)^{12} - (\sigma/r)^6] , \tag{3}$$

where ϵ is the depth of the potential and σ is the ("collision") separation at which the potential vanishes. Choosing $\epsilon/k = 119.8$ K and $\sigma = 3.405$ Å brings the potential (3) into rough correspondence with argon in its normal liquid range.

A host of equilibrium[11] and nonequilibrium[12] simulations (both Monte Carlo and molecular dynamics) have been carried out for the Lennard-Jones potential so that the pressure, energy, viscosity, bulk viscosity,[13] and thermal conductivity can be regarded as relatively well-known functions of the density and temperature; i.e., $P(\rho, T)$, $E(\rho, T)$, $\eta(\rho, T)$, $\eta_v(\rho, T)$, and $\kappa(\rho, T)$ are known.

In fixed-temperature Monte Carlo simulations,

thermodynamic pressure and energy are determined by evaluating phase-space averages of the virial and Hamiltonian. In fixed-energy equilibrium molecular dynamics simulations, the time averages of the virial and the temperature (from kinetic energy) provide equivalent thermodynamic information. Transport coefficients can be determined by applying the results of Green-Kubo fluctuation theory to equilibrium molecular dynamics simulations. Alternative methods, using nonequilibrium molecular dynamics, have been developed in order to measure transport coefficients more directly. Heat reservoirs maintained at two different temperatures produce a dynamical heat current, from which the thermal conductivity can be inferred. Momentum reservoirs maintained at two different velocities generate a shear stress, from which the shear viscosity follows. Both viscosities, bulk and shear, can be determined by a recent modification of nonequilibrium molecular dynamics.[13] In these calculations a Hamiltonian coupling the strain rate tensor ∇u with Doll's tensor $\Sigma q p$ provides dissipative equations of motion. Numerical solutions incorporating the dissipation give estimates for both viscosity coefficients.

Figure 3 illustrates the similarity between the numerically generated phase diagram for the Lennard-Jones potential and the actual one for argon. We have also indicated in that figure the density-temperature states traversed by the two Klimenko-Dremin[5] shock waves and the stronger one described in the next three sections. Better agreement with argon data can be obtained by using a more complicated pair potential,[14] but for simplicity we use the potential (3). An even simpler form of interaction, the inverse-12th-power "soft-sphere" repulsive potential has been studied
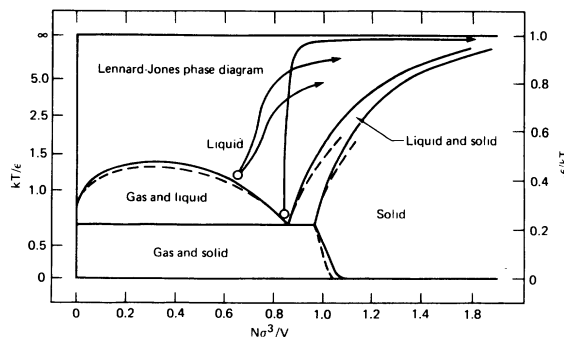

FIG. 3. Phase diagrams for the Lennard-Jones potential and for argon. The density-temperature trajectories for the two shock waves treated in Ref. 6 and the stronger shock treated here are shown as arrows. The initial states are the open circles and the final states the arrow heads.

exhaustively[11,15] and provides convenient high-temperature limiting forms for the Lennard-Jones constitutive properties.

Ree built upon Hansen's ideas to construct an accurate representation of the Helmholtz free energy of the fluid for the Lennard-Jones potential, from which both the pressure and the internal energy can be found by differentiation. Ree's fluid free energy appears in Appendix A. The corresponding representations for transport properties appear in Appendix B. The qualitative dependence of the constitutive properties on density and temperature is illustrated in Fig. 4.

IV. MACROSCOPIC SHOCK-WAVE STRUCTURE

A shock wave linking the Lennard-Jones liquid at $N\sigma^3/V = 0.8442$ and $kT/\epsilon = 0.722$, near the triple point, to a hot dense fluid at $N\sigma^3/V = 1.571$, $kT/\epsilon = 100$, can be generated by using a piston velocity of $22.4(\epsilon/m)^{1/2}$. The resulting shock wave travels at $u_s = 48.5 \ (\epsilon/m)^{1/2}$. Using here, and in what follows, units of m, σ, and ϵ for mass, distance, and energy, the pressure increases from 0 to 917 and the per particle energy from −5 to 246. These data result from a numerical iterative solution of the Hugoniot equation (2) using Ree's equation of state
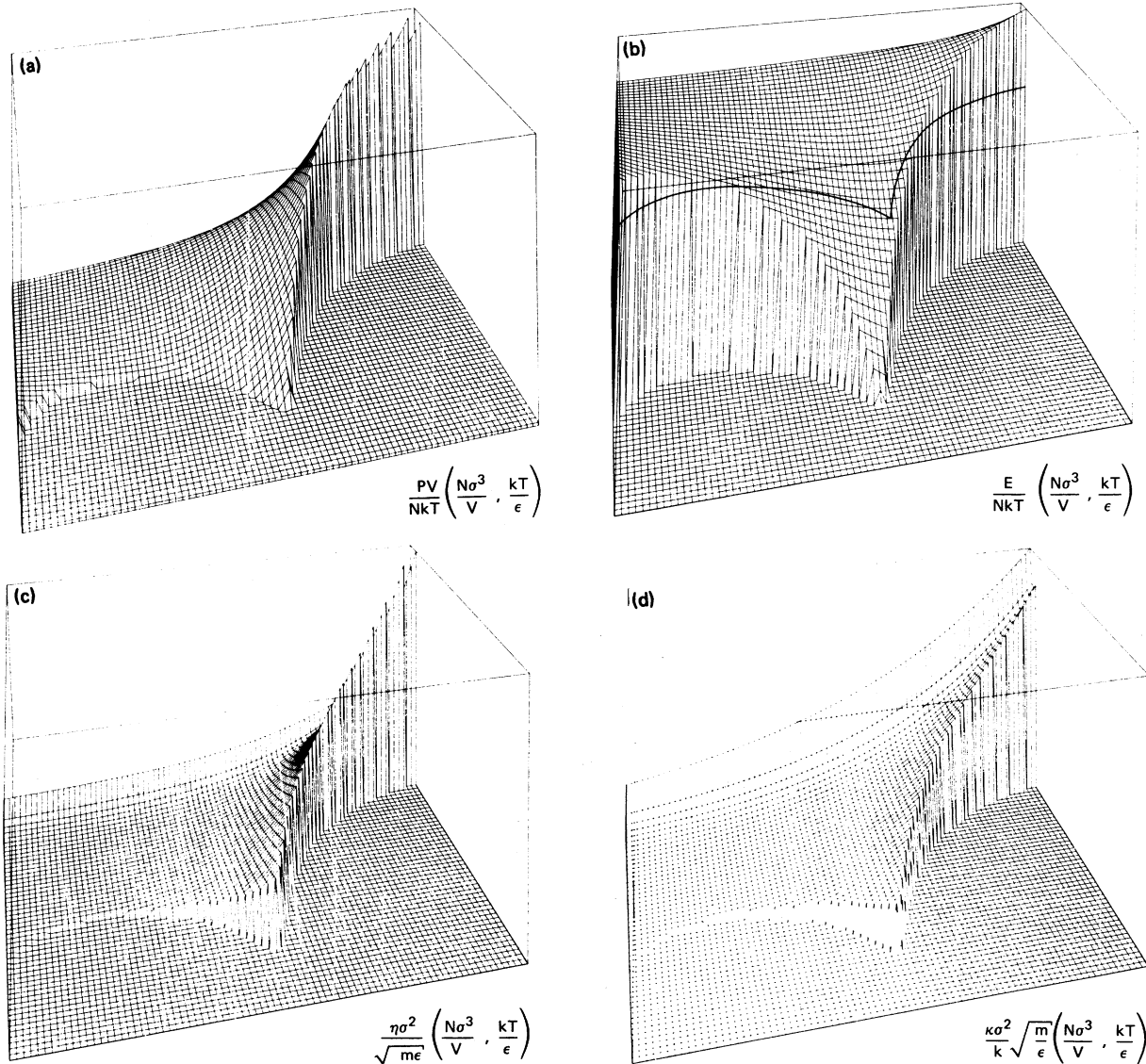

FIG. 4. Pressure, energy, shear viscosity, and thermal conductivity for the Lennard-Jones potential. The independent variables, $\exp(-\epsilon/kT)$ and $N\sigma^3/V$ span a temperature range $0 < kT/\epsilon < 100$ and a reduced density range $0 < N\sigma^3/V < 1.60$. The dependent variables span the ranges $0 < PV/NkT < 16$, $-8 < ENkT < 3.5$, $0 < \eta\sigma^2(m\epsilon)^{-1/2} < 50$, and $0 < \kappa\sigma^2(m/\epsilon)^{1/2}/k < 60$.

from Appendix A. To calculate the shock-wave profile the conservation equations within the shock must be solved:

$$\rho u = 40.9\,,$$

$$P_{eq} - (\eta_v + \tfrac{4}{3}\eta)\,\frac{du}{dx} + \rho u^2 = 1980 = P_{xx} + \rho u^2\,, \qquad (4)$$

$$\rho u\left(E_{eq} + \frac{P_{xx}}{\rho} + \frac{u^2}{2}\right) - \kappa\frac{dT}{dx} = 47\,900\,.$$

The calculation proceeds in two steps.[16] See Appendix C. The first of these equations is used to express u and du/dx in terms of ρ and $d\rho/dx$, giving two coupled equations for $d\rho/dx$ and dT/dx. These are combined, giving a single differential equation for $d\rho/dT$, which can be solved numerically,[17] beginning at the hot (shocked) thermodynamic state. The result of this integration is the density-temperature relation shown in Fig. 3, and in more detail in Fig. 5. Once density and temperature are related, then the momentum and the energy equations in (4) can be used to find these variables as functions of coordinate through the shock wave. To solve the equations it is essential, of course, that the equilibrium pressure, energy, and transport coefficients be known functions of density and temperature.

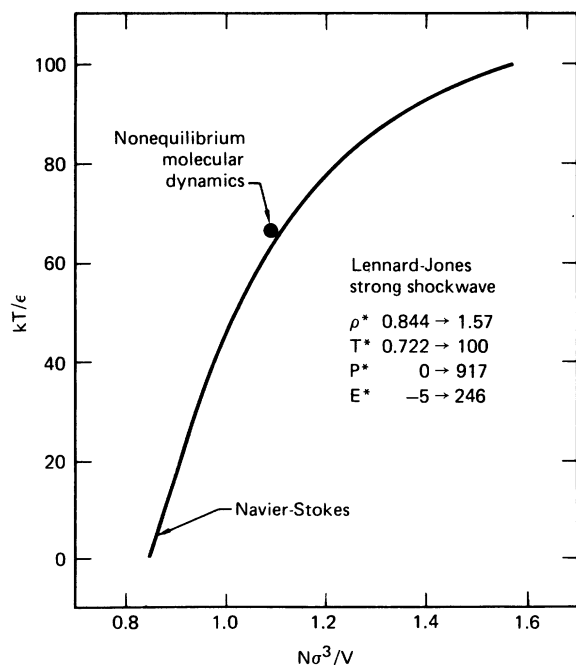The continuum profiles found are sketched in Fig. 6. The relative change in each of the thermo-

dynamic quantities can be represented fairly well as $\tfrac{1}{2}\tanh(2x/\lambda)$, where λ characterizes the shock width for the variable in question. The widths obtained, from density, pressure, and temperature, respectively, are 1.0, 1.1, and 0.83, where in each case the change in the variable is divided by the maximum x derivative to find the corresponding "width." Just as in the zero-density solutions of the Boltzmann equation, our high-density results show that the temperature rises ahead of

FIG. 5. Density-temperature states traversed in the shock wave according to continuum mechanics are shown as a full curve. The ● indicates the state at the shock-wave center according to 4800-particle nonequilibrium molecular dynamics.
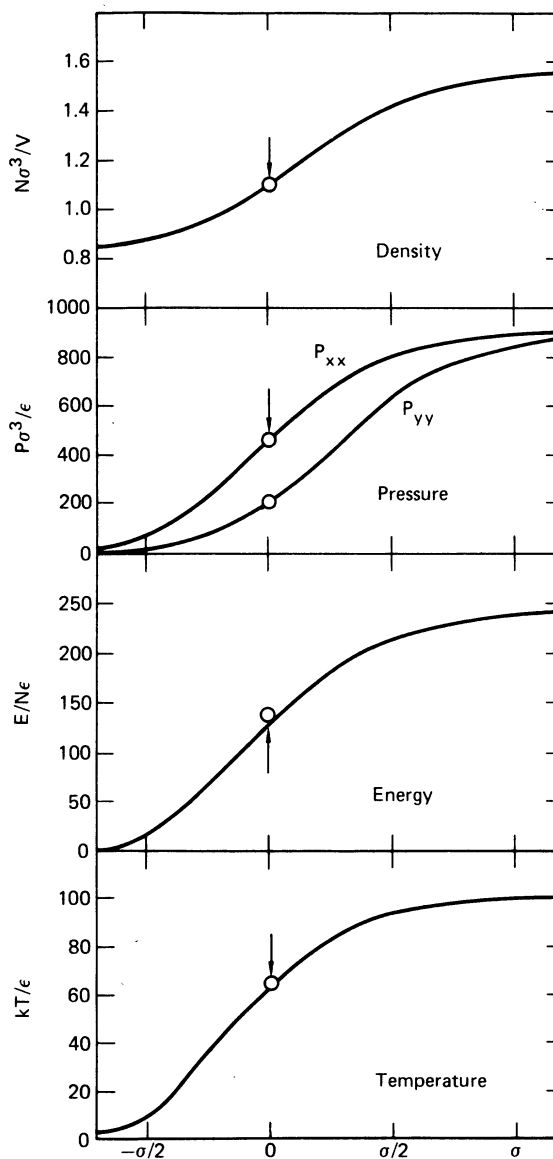

FIG. 6. Density, stress, energy, and temperature profiles from continuum mechanics, using the constitutive model described in the appendices. The circles indicate values from the molecular dynamics simulation. The agreement for density and P_{xx} is assured by mass and momentum conservation.

the density while the equilibrium pressure rises behind. Profiles of the gradients of the thermodynamic variables show that the temperature gradient is relatively asymmetric, rising more steeply than it falls.. In Table I we list the Navier-Stokes properties at the shock "center" arbitrarily chosen as the point where the laboratory frame speed is $-\frac{1}{2}u_p$ (so that u is $u_s - \frac{1}{2}u_p$ in the comoving frame). In Sec. V we obtain corresponding profiles from solutions of the atomic equations of motion.

V. MICROSCOPIC SOLUTION

The simplest way to simulate a shock wave with molecular dynamics is to shrink the periodic system size unaxially, as indicated in Fig. 7. The left and right boundaries of the system move with x velocities of $\pm u_p$ so that the right boundary plays the role of the piston in the topmost part of Fig. 2. The result is a pair of shock waves moving symmetrically toward the central plane away from the two boundaries. The velocities of the shock waves agree with the estimate from Ree's equation of state, 48.5.

Dependence of the shock structure on system size was checked by considering systems with equivalent cross sections of 25.4 σ^2 and 45.1 σ^2. Profiles of velocity, density, stress, energy, and temperature were accumulated by summing the corresponding particle properties for all particles into bins moving at velocity u_s (laboratory frame). These profiles are shown in Fig. 8. Both the longitudinal and transverse temperatures, as well as the corresponding kurtoses $(\langle \delta V^4 \rangle - 3 \langle \delta V^2 \rangle^2)$, are included in Fig. 9 to characterize the nonequilibrium velocity distribution. A more careful division of pair-force contributions to stress and energy might lead to smoother profiles. A comparison of profiles for different time intervals established that the statistical uncertainties are of the same order as the post-shock ripples seen in Fig. 8.

The effect of the bin size d on the apparent width Λ of the profiles can be estimated by a simple hyperbolic-tangent approximation[18] with a true width of λ estimated for the function

TABLE I. Comparison of fluid properties at the shock center from molecular dynamics (MD) and from Navier-Stokes (NS) continuum mechanics. All the data correspond to a density of 1.098 with $P_{xx} = 459$. The mass, momentum, and energy fluxes are given in Eq. (4) of the text.

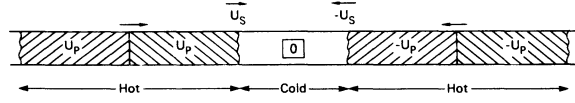|	$\langle P \rangle$	P_{yy}	P_{eq}	E	T	T_{xx}	T_{yy}	η	η_v	κ
MD	303	225		138	67	100	50	7.3	1.9	46
NS	297	216	267	127	64			5.3	1.3	28

FIG. 7. Boundary conditions used to generate a shock wave with nonequilibrium molecular dynamics.

$$f(x) = \tfrac{1}{2}\tanh(2x/\lambda), \quad f'(0) = \lambda^{-1}. \tag{5}$$

The apparent width is then given by

$$\Lambda^{-1}(d,\lambda) = \left(\frac{1}{d} \int_0^d f\, dx - \frac{1}{d} \int_{-d}^0 f\, dx \right) \Big/ d$$

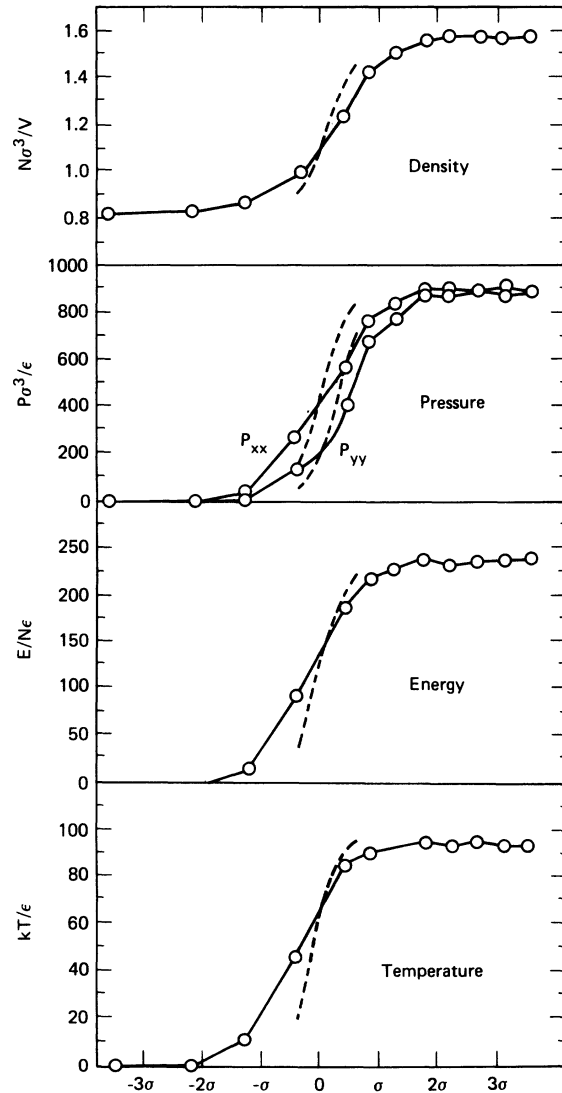$$= \frac{\lambda}{2d^2} \ln \cosh(2d/\lambda). \tag{6}$$

FIG. 8. Density, stress, energy, and temperature profiles from nonequilibrium molecular dynamics. Corresponding Navier-Stokes results from Fig. 6 are shown as dashed lines. The molecular dynamics data were generated using a bin width of 0.65 σ.
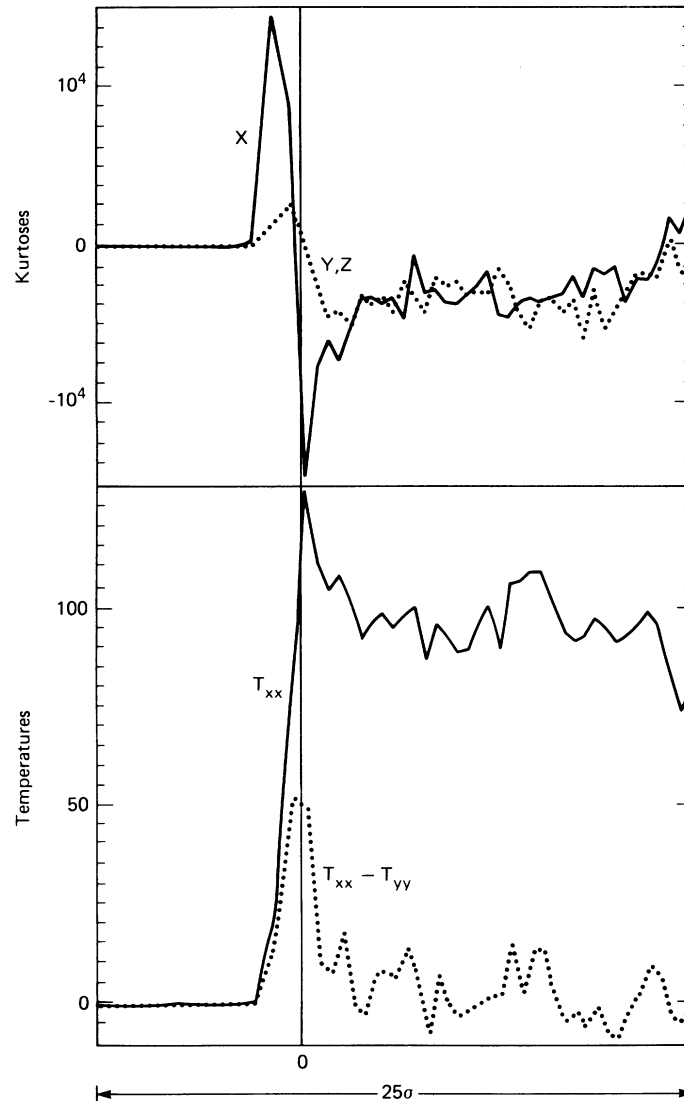
FIG. 9. Velocity kurtoses $\langle\delta V^4\rangle - 3\langle\delta V^2\rangle^2$, longitudinal, and transverse temperature profiles from 4800-particle non-equilibrium molecular dynamics.

For bin sizes smaller than the apparent width Λ the true shock width is, to second order, $\lambda = \Lambda - (2d^2/3\Lambda) + \cdots$. From the measured velocity profile, Λ, d, and λ are, respectively, 1.58, 0.65, and 1.40.

The computed profiles are in good agreement with the conservation relations for mass and momentum,

$$\rho u = 40.9, \quad P_{xx} + \rho u^2 = 1980.$$

The energy flux, 47 900, was not measured directly but is required in order to estimate the heat flux from energy conservation.

The shapes of the profiles are described well by the Mott-Smith form (5). The flow properties at the shock center appear in Table I. A comparison

of the continuum and atomistic profiles is given in Sec. VI.

VI. COMPARISON OF MACROSCOPIC AND MICROSCOPIC SHOCK WAVES

We limit our comparison to the plane described in Table I, at which the particle velocity has reached half the final value u_p: $u = u_s - (u_p/2) = 37.3$. The conservation relations show that ρ is 1.098 and P_{xx} is 459 at this plane. The atomistic profile of $P_{xx} - P_{yy}$ is difficult to interpolate for a maximum. We use instead as primary data the values of the mean pressure 303 and internal energy 138. These establish that P_{yy} is 225 and that the heat flux is −3200. The shock width, estimated in Sec.

V from the measured velocity profiles, (though the temperature width is probably slightly smaller, we cannot estimate a significant difference) is 1.40, giving velocity and temperature gradients of 16 and 71, respectively.

From these data the atomistic Newtonian viscosity coefficients and heat conductivity are estimated, using a temperature of 67 corresponding to an equilibrium pressure of 273,

$$\eta = 7.3, \quad \eta_v = 1.9, \quad \kappa = 46.$$

The transport coefficients estimated from Appendix B are all somewhat smaller (5.3, 1.3, and 28) and the discrepancies lie outside the uncertainty in the shock width. A slightly smaller width, given larger gradients would lead to good agreement for all three coefficients. See Fig. 8.

The Navier-Stokes equations omit two kinds of information available from the atomistic simulations: The difference between the longitudinal and transverse temperatures and the non-Maxwellian character of the velocity distribution. Both of these features appear in the molecular dynamics simulations, as illustrated in Fig. 9, and neither is yet understood from a theoretical standpoint. There is no reason why a linear theory describing the decay of differences between longitudinal and transverse temperatures could not be developed. On the other hand, the kurtoses functions shown in Fig. 9 which describe the non-Maxwellian shape of the longitudinal and transverse velocity distribution certainly lie outside the usual realm of continuum mechanics, where local thermodynamic equilibrium is assumed. The Mott-Smith bimodal velocity distribution[18] provides a simple recipe for the kurtosis of a shock wave, but that recipe does not agree with the results shown in Fig. 9. Moreover, the mean temperature T $= \frac{1}{3}(T_{xx} + T_{yy} + T_{zz})$ as a function of position in the molecular dynamics shock wave does not have a peak through the profile, as is predicted by the Mott-Smith model. Therefore, even though the Navier-Stokes assumption of an isotropic Maxwellian (equilibrium) velocity distribution is incomplete for a shock wave in a fluid, we conclude that this picture is more satisfactory than the Mott-Smith recipe (the bimodal velocity distribution).

The main conclusion that can be drawn from this work, taking into account the relatively good agreement already found for lower compressions, is that nonequilibrium molecular dynamics shock-wave experiments can be described reasonably well by Navier-Stokes hydrodynamics. The Navier-Stokes shock waves are evidently a little too narrow. Moreover, in the continuum description of the heat flux, no account is taken of the

kinetic energy analog of the shear stress, namely, the "shear temperature," or anisotropy of the velocity distribution through the shock front.

Another interpretation of these results is the supposition that the fluctuations about equilibrium in an atomistic fluid generate, on the local level, gradients and strain rates almost as large as those seen in shock waves. Fluctuations about local thermodynamic equilibrium decay on short time scales by collisions and on longer time scales by hydrodynamic Navier-Stokes modes, where the transport coefficients are obtained from appropriate Green-Kubo autocorrelation functions. The Navier-Stokes transport coefficients have also been obtained from nonequilibrium steady-state experiments, and because these coefficients describe shock waves quite well, further weight is lent to the supposition that the states achieved by a fluid element in a nonequilibrium shock-wave experiment are not very far from equilibrium. This means that shock-wave simulations in the fluid phase can be used to obtain reasonable estimates for the transport coefficients, without the need for special reservoirs and requiring only relatively simple nonequilibrium boundary conditions.

In closing, we note that earlier investigators have studied strong shock waves in the ideal-gas low-density high-temperature limit by solving an approximate Boltzmann equation.[19] Just as in the case of dense-fluid shock waves, they find that the position $x = u_s t$ in the steady profile, where the particle velocity reaches half of its final value, is very close to the point of maximum particle-velocity gradient. Also, just as in the dense-fluid case, they find that the Navier-Stokes approximation is quite good for ideal-gas shock waves, with more noticeable discrepancies at higher shock-wave strengths. Unlike the dense-fluid case however, the ideal-gas shock wave deviates significantly from the Navier-Stokes solution only in the upstream (cold) part of the profile, where x is less than $u_s t$ and the ratio of shear stress to mean stress is not negligible.

Just why the agreement is as good as it is over such a wide range of fluid conditions has not been explained.[20] Theoretical efforts to go beyond the Navier-Stokes level have not been completed yet.

APPENDIX A

The Helmholtz free energy, minus the ideal-gas contribution, for a Lennard-Jones 6-12 fluid has been fit to an analytical form by Hansen and Ree.[21]

$$A^e/NkT = +3.629x + 3.632x^2 + 3.4975x^3 + 2.865x^4 + 0.2176x^{10}$$
$$- (\epsilon/kT)^{1/2}(5.369x + 6.580x^2 + 6.175x^3 - 4.269x^4 + 1.864x^5)$$
$$+ (\epsilon/kT)(-3.492x + 9.349x^2 - 11.835x^3 + 7.954x^4 - 2.239x^5),$$

where $x = (N\sigma^3/V)(\epsilon/kT)^{1/4} = (\rho\sigma^3/m)(\epsilon/kT)^{1/4}$. The equation of state is obtained by differentiation; the pressure P is given by

$$PV/NkT = Pm/\rho kT = 1 + \rho\left(\frac{\partial(A^e/NkT)}{\partial\rho}\right)_T ,$$

and the internal energy per unit mass E by

$$Em = \tfrac{3}{2}NkT + \left(\frac{\partial(A^e/NkT)}{\partial(1/NkT)}\right)_\rho .$$

When a shock wave passes through the fluid, the initial and final states are related by Eqs. (1) and (2) of the text, the Hugoniot relations. Suppose, for example, that we wish to compute the final density ρ_1 and the velocities of the piston u_p and the shock wave u_s, given the initial and final temperatures, T_0 and T_1, and the initial density ρ_0. The above equation of state yields the initial pressure, $P_0 = P(\rho_0, T_0)$, and internal energy, $E_0 = E(\rho_0, T_0)$. By searching for the zero of the function

$$\Delta(\rho) = E(\rho, T_1) - E_0 - \tfrac{1}{2}[P(\rho, T_1) + P_0](1/\rho_0 - 1/\rho) ,$$

the final density $\rho = \rho_1 > \rho_0$ can be found, for which $P_1 = P(\rho_1, T_1)$ and $E_1 = E(\rho_1, T_1)$. The momentum conservation equation then yields

$$u_p = [(P_1 - P_0)(1/\rho_0 - 1/\rho_1)]^{1/2} ,$$

and the mass conservation equation gives

$$u_s = u_p/(1 - \rho_0/\rho_1) .$$

APPENDIX B

The transport coefficients for the Lennard-Jones potential have been discussed by Ashurst,[22] who gives an analytic representation of the collision integral necessary for the low-density thermal conductivity and shear viscosity. This same integral is tabulated in Hirschfelder, Curtiss, and Bird.[8] The excess shear viscosity has the form

$$\Delta\eta(m\epsilon)^{-1/2}(\epsilon/kT)^{2/3}\sigma^2$$
$$= 0.0152[1 - 0.5(\epsilon/kT)^{1/2} + 2(\epsilon/kT)](e^{bx} - 1) ,$$

where $b = 7.02 [1 - 0.2(\epsilon/kT)^{1/2}]$.

The form for the thermal conductivity given in Ashurst's report cannot be used at low temperatures, near the triple point, so we have used the simpler representation[12]

$$\Delta\kappa(m/\epsilon)^{1/2}(\epsilon/kT)^{2/3}\sigma^2/k = 0.36[\exp(3.76x) - 1].$$

This relatively crude approximation is justified by (1) the relatively greater uncertainty in the Lennard-Jones thermal conductivity and (2) the relative insensitivity of shock-wave structure to the conductivity.

The bulk viscosity for the Lennard-Jones potential is known less well. Data for the high-temperature limit and triple point show that the bulk viscosity, unlike the shear viscosity, varies by an order of magnitude even when expressed in terms of soft-sphere scaling variables. Because our interest here has primarily been high temperatures (the reduced temperature at the shock center is 67) we have used an empirical form chosen to fit the soft-sphere data and the results given in Table II:

$$\eta_v\sigma^2(\epsilon/kT)^{2/3}(m\epsilon)^{-1/2} = 0.31x^{3/2}\exp[0.13(\epsilon/kT)^{1/4}].$$

APPENDIX C

Time t can be eliminated from the (X, t) dependence of the hydrodynamic field variables (ρ, u, P_{xx}, E), if the shock wave is steady, by transforming the laboratory coordinate X to a comoving frame coordinate

$$x = X + u_s t ,$$

where u_s is the shock-wave velocity. The fluxes of mass, momentum, and energy are then [see Eq. (1) of the text]

$$\rho(x)u(x) = \rho_0 u_0 ,$$

$$P_{xx}(x) + \rho(x)u^2(x) = P_0 + \rho_0 u_0^2 ,$$

$$\left(E(x) + \frac{P_{xx}(x)}{\rho(x)} + \tfrac{1}{2}u^2(x)\right)\rho(x)u(x) + q(x)$$

$$= \left(E_0 + \frac{P_0}{\rho_0} + \tfrac{1}{2}u_0^2\right)\rho_0 u_0 .$$

TABLE II. Lennard-Jones bulk viscosities. These data were obtained as described in Ref. 13, solving modified Newtonian (second-order) equations of motion and using a one-dimensional strain amplitude of 0.02. The soft-sphere inverse-12th-power bulk viscosities from Ref. 13 correspond to reduced (last column) viscosities of 0.08 at $x = 0.4$ and 0.13 at $x = 0.6$, suggesting that attractive forces increase the bulk viscosity at high temperature. All of these calculations were carried out with 54 particles. The density, temperature, reduced density x, frequency of oscillation, number of cycles, and reduced bulk viscosity are all listed.

$N\sigma^3/V$	kT/ϵ	x	$\omega\sigma(m/\epsilon)^{1/2}$	cycles	$\eta_v\sigma^2(m\epsilon)^{-1/2}$	$[\eta_v\sigma^2/(m\epsilon)^{1/2}](\epsilon/kT)^{2/3}$
0.8	16	0.4	50	200	0.69 ± 0.05	0.11
1.2	81	0.4	25	100	$1.9\ \pm0.3$	0.10
1.2	81	0.4	100	200	$2.2\ \pm0.2$	0.12
1.6	256	0.4	250	200	$3.9\ \pm0.3$	0.10
2.0	625	0.4	200	400	$7.6\ \pm0.7$	0.10
2.0	625	0.4	400	200	$6.7\ \pm0.6$	0.09
1.2	16	0.6	50	200	1.24 ± 0.1	0.20
1.8[a]	81	0.6	100	200	$3.4\ \pm0.4$	0.18
1.8[a]	81	0.6	100	600	$2.7\ \pm0.2$	0.14

[a] These two calculations were carried out using two independent methods. The longer run, from a CRAY, used an ordinary differential equation solver to solve Hamiltonian (first-order) equations of motion. The shorter run, from a CDC 7600, and the other results given here used the Newtonian equations of motion discussed in Ref. 13, and required a somewhat smaller time step.

The Navier-Stokes constitutive relation is

$$P_{xx}(x) = P(x) - \eta_L(x)\frac{du(x)}{dx},$$

where P is the isotropic equilibrium pressure and $\eta_L = \eta_V + \frac{4}{3}\eta$; Fourier's law for heat conduction is

$$q(x) = -\kappa(x)\frac{dT(x)}{dx}.$$

By the mass flux equation, velocity can be expressed in terms of the density

$$u(x) = \frac{\rho_0 u_0}{\rho(x)}, \quad \frac{du(x)}{dx} = -\frac{\rho_0 u_0}{\rho^2(x)}\frac{d\rho(x)}{dx}.$$

Velocity can then be eliminated from the momentum and energy equations and the gradients of density and temperature evaluated:

$$\frac{d\rho(x)}{dx} = \frac{\rho_0 u_0}{\eta_L(x)}\left(\frac{\rho^2(x)}{\rho_0^2 u_0^2}[P_0 - P(x)] + \frac{\rho^2(x)}{\rho_0} - \rho(x)\right).$$

$$\frac{dT(x)}{dx} = \frac{\rho_0 u_0}{\kappa(x)}\left[E(x) - E_0 + P_0\left(\frac{1}{\rho(x)} - \frac{1}{\rho_0}\right) + \frac{1}{2}u_0^2\left(\frac{2\rho_0}{\rho(x)} - \frac{\rho_0^2}{\rho^2(x)} - 1\right)\right].$$

Hence,

$$\frac{d\rho}{dT}(x) = \frac{d\rho(x)/dx}{dT(x)/dx} = \frac{\kappa(x)}{\eta_L(x)}\ \frac{\rho^2(x)/\rho_0^2 u_0^2[P_0 - P(x)] + \rho^2(x)/\rho_0 - \rho(x)}{E(x) - E_0 + P_0[1/\rho(x) - 1/\rho_0] + \frac{1}{2}u_0^2[2\rho_0/\rho(x) - \rho_0^2/\rho^2(x) - 1]}.$$

In order to integrate this equation, we must assume that the temperature can be expressed as a unique function of density,

$$T(x) = T[\rho(x)],$$

so that the functions $f = P$, E, η_L, and κ can be written as

$$f(x) = f[\rho(x), T(x)] = f(\rho),$$

whereupon $d\rho/dT$ can be integrated self-consistently. The numerator and denominator of the right side of the equation for $d\rho/dT$ both vanish at the initial and final states of the shock wave by the Hugoniot relations [Eqs. (1) and (2) of the text]. However, by expanding in a Taylor series in density about the initial ($i = 0$) or final ($i = 1$) state, we obtain

a finite result,

$$\left.\frac{d\rho}{dT}\right|_i = \frac{\kappa(\rho_i, T_i)}{\eta_L(\rho_i, T_i)}\ \frac{\rho_i[c_T^2(\rho_i, T_i)u_i^{-2} - 1]}{\beta(\rho_i, T_i)c_T^2(\rho_i, T_i)T_i},$$

where β is the thermal expansion coefficient

$$\beta = -\frac{1}{\rho}\left(\frac{\partial\rho}{\partial T}\right)_P,$$

c_T is the isothermal sound speed

$$c_T^2 = \left(\frac{\partial P}{\partial\rho}\right)_T,$$

and

$$u_0 = u_s, \quad u_1 = u_s - u_p.$$

[1]For a guide to the review literature, see L. Davison and R. A. Graham, Phys. Rep. 55, 255 (1979).

[2]M. Ross, W. Nellis, and A. Mitchell, Chem. Phys. Lett. 68, 532 (1979).

[3]A. C. Mitchell and W. J. Nellis, in *High-Pressure Science and Techology*, 1, edited by K. D. Timmerhaus and M. S. Barber (Plenum, New York, 1979).

[4]C. E. Ragan III, Phys. Rev. A 21, 458 (1980).

[5]V. Y. Klimenko and A. N. Dremin, in *Detonatsiya, Chernogolovka*, edited by O. N. Breusov et al. (Akad. Nauk, Moscow, 1978), p. 79.

[6]W. G. Hoover, Phys. Rev. Lett. 42, 1531 (1979).

[7]R. Courant and K. O. Friedrichs, *Supersonic Flows and Shock Waves* (Interscience, New York, 1948).

[8]J. O. Hirschfelder, C. F. Curtiss, and R. B. Bird, *Molecular Theory of Gases and Liquids* (Wiley, New York, 1954), pp. 783–797.

[9]For a recent atomistic solid-phase shock-wave simulation see B. L. Holian and G. K. Straub, Phys. Rev. Lett. 43, 1598 (1979). Both fluid and solid simulations have also been carried out at the National Bureau of Standards. See D. H. Tsai and R. A. McDonald, High Temp. High Pressures 8, 403 (1976).

[10]*Physics of Simple Liquids*, edited by H. N. V. Temperley, J. S. Rowlinson, and G. S. Rushbrooke (North-Holland, Amsterdam, 1968).

[11]D. Levesque and L. Verlet, Phys. Rev. 182, 307 (1969); J. P. Hansen, Phys. Rev. A 2, 221 (1970).

[12]W. T. Ashurst, Ph.D. thesis, University of California, Davis, 1975 (unpublished); D. Levesque, L. Verlet, and J. Kurkijarvi, Phys. Rev. A 7, 1690 (1973); W. G. Hoover, D. J. Evans, R. B. Hickman, A. J. C. Ladd, W. T. Ashurst, and B. Moran, Phys. Rev. A 22, 1714 (1980).

[13]W. G. Hoover, A. J. C. Ladd, R. B. Hickman, and B. L. Holian, Phys. Rev. A 21, 1756 (1980).

[14]J. A. Barker, R. A. Fisher, and R. O. W. Watts, Mol. Phys. 21, 657 (1971).

[15]W. G. Hoover, M. Ross, K. W. Johnson, D. Henderson, J. A. Barker, and B. C. Brown, J. Chem. Phys. 52, 4931 (1970); J. N. Cape, Ph.D. dissertation, Cambridge University, 1979 (unpublished).

[16]D. Gilbarg and D. Paolucci, J. Rat. Mech. Anal. 2, 617 (1953); L. M. Schwartz and D. F. Hornig, Phys. Fluids 6, 1669 (1963).

[17]A. C. Hindmarsh, Lawrence Livermore Laboratory Report No. UCID-30 001 (unpublished), Revision 3 (1974).

[18]H. M. Mott-Smith, Phys. Rev. 82, 885 (1951); H. Salwen, C. E. Grosch, and S. Ziering, Phys. Fluids 7, 180 (1964).

[19]G. E. Uhlenbeck, Annu. Rev. Fluid Mech. 12, 1 (1980).

[20]H. W. Liepmann, R. Narasimha, and M. T. Chahine, Phys. Fluids 5, 1313 (1962).

[21]F. H. Ree, J. Chem. Phys. (in press).

[22]W. T. Ashurst, Sandia Livermore Laboratory Report No. SAND 76-8710, 1976 (unpublished).